On some deficiencies of the AUFS scheme for Euler flows and possible fixes

Friedemann Kemm

Institute for Applied Mathematics and Scientific Computing, Brandenburgische Technische Universität Cottbus, Konrad-Wachsmann-Allee 1, 03046 Cottbus, Germany

Abstract

The AUFS-scheme by Sun and Takayama is a flux splitting scheme without breakdown of discrete shock profiles, usually called carbuncle, but still with a fine resolution of entropy waves. Unfortunately, in numerical tests, the viscosity on entropy waves turns out to be too small and the viscosity on shear waves to be too high. In this paper, we provide fixes to overcome these deficiencies.

Keywords: Flux Vector Splitting, Carbuncle, Positivity of Pressure, Gas Dynamics, inviscid, contact and shear waves
2000 MSC: 35L65, 65M06, 76L05, 76M12, 76N15

1. Introduction

In their original paper, Steger and Warming [1] present not only a splitting of the Euler flux into a left- and a right-going part but also a more general framework which allows to split the flux function itself into different parts. As an example [1, p. 271], they propose the following splitting of the 1d-Euler flux

$$\boldsymbol{f}(\boldsymbol{q}) = u\,\boldsymbol{q} + \boldsymbol{P}(\boldsymbol{q}) = u \begin{pmatrix} \rho \\ \rho u \\ E \end{pmatrix} + \begin{pmatrix} 0 \\ p \\ pu \end{pmatrix} \tag{1}$$

with the wave speeds for the advective flux $u\,\boldsymbol{q}$ assumed to be u, u, u and for the central part, the pressure part, $\boldsymbol{P}(\boldsymbol{q})$ assumed to be $0, \pm c$ with the speed of sound c. Although these are not the actual eigenvalues of the according flux-Jacobians – the Jacobian for the advective part is not even diagonalizable, and the eigenvalues for the central part are $0, \pm\sqrt{\frac{\gamma-1}{\gamma}}\,c$ – together with their numerical

flux formula (4.19), this leads to a usable numerical scheme. For the 2d-case, the numerical viscosity of the central part then reads as

$$\delta \boldsymbol{Q}_{\mathrm{SW}} = \frac{1}{2c_l} \begin{pmatrix} p_l \\ u_l p_l \\ v_l p_l \\ H_l p_l \end{pmatrix} - \frac{1}{2c_r} \begin{pmatrix} p_r \\ u_r p_r \\ v_r p_r \\ H_r p_r \end{pmatrix}, \tag{2}$$

where the subscripts refer to the left and right state. Thus, the numerical flux can be written as

$$\boldsymbol{g}(\boldsymbol{q}_l, \boldsymbol{q}_r) = \bar{u}\boldsymbol{q}_{up} + \frac{1}{2}(\boldsymbol{P}_l + \boldsymbol{P}_r) + \delta \boldsymbol{Q}_{\mathrm{SW}} \tag{3}$$

with some averaged advection speed $\bar{u}$. The subscript up denotes the upwind value, e. g. for $\bar{u} > 0$ the left state.

Sun and Takayama [2] modify this scheme in two ways. First, they introduce some upwinding to the central part by

$$\boldsymbol{g}(\boldsymbol{q}_l, \boldsymbol{q}_r) = \bar{u}\boldsymbol{q}_{\mathrm{up}} + M\boldsymbol{P}_{\mathrm{up}} + (1 - M)\left(\frac{1}{2}(\boldsymbol{P}_l + \boldsymbol{P}_r) + \delta \boldsymbol{Q}_{\mathrm{SW}}\right), \tag{4}$$

where M is an estimate for the local Mach-number. Second, they replace the left and right speed of sound in the denominators of (2) by an averaged speed of sound $\bar{c}$ to get

$$\delta \boldsymbol{Q}_{\mathrm{ST}} = \frac{1}{2\bar{c}} \begin{pmatrix} p_l - p_r \\ p_l u_l - p_r u_r \\ p_l v_l - p_r v_r \\ \frac{\bar{c}^2}{\gamma-1}(p_l - p_r) + \frac{1}{2}(p_l u_l^2 - p_r u_r^2) \end{pmatrix}. \tag{5}$$

As a justification for that, they argue that for an isentropic gas, the left and right speed of sound are the same, and both numerical viscosities would coincide with that for a Rusanov-type scheme

$$\delta \boldsymbol{Q}_{\mathrm{Rus}} = \frac{\bar{c}}{2} \begin{pmatrix} \rho_l - \rho_r \\ \rho_l u_l - \rho_r u_r \\ \rho_l v_l - \rho_r v_r \\ E_l - E_r \end{pmatrix}. \tag{6}$$

For an ideal (or even a real) gas, however, their choice for the viscosity $\delta \boldsymbol{Q}_{\mathrm{ST}}$ differs from the others in one important point: in the absence of pressure and
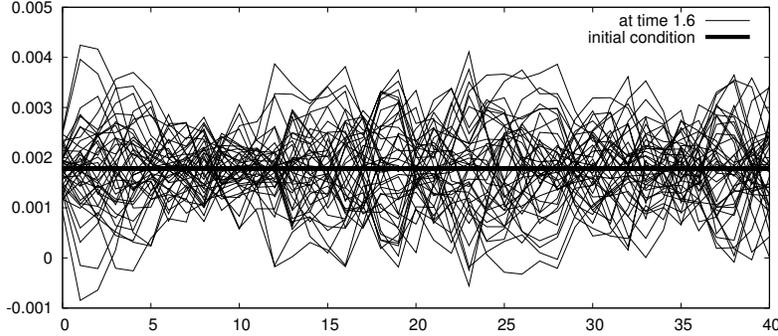
2

Figure 1: Pressure in the supersonic region of the steady shock test at $t = 16$ when computed with original AUFS.

velocity jumps, it completely vanishes. Thus, the resulting method exactly resolves any pure entropy wave. At a first glance this is an appealing property, which, as is shown in their paper [2], leads to high resolution in many test cases. But this is not without risk. As Gressier, Villedieu, and Moschetta [3] proof, for FVS-schemes, there is an inherent incompatibility between the exact resolution of entropy waves and positivity. The consequences can be seen in Figure 1. There, the supersonic part of the steady shock test, introduced by Dumbser et al. [4] to test numerical schemes for their tendency to evolve a carbuncle, is shown. The test starts with a strong steady shock and small randomized numerical noise added to the primitive variables. After a short time, the original AUFS-scheme produces negative pressure.

Another issue of the AUFS-scheme is the third component of the viscosity $\delta\boldsymbol{Q}$. In a shear wave, for all variants, i. e. (2), (5), and (6), it only vanishes if the shear wave is trivial, i. e. if there is no jump in the tangential velocity v. On the one hand, this seems to be the main reason why AUFS does not show the carbuncle. On the other hand, it leads to a poor resolution of boundary layers. As can be seen from Section 3.6, the resolution for the original AUFS is even poorer than with $\delta\boldsymbol{Q}_{\mathrm{SW}}$.

In this paper, we investigate the loss in the resolution of entropy waves that results from using $\delta\boldsymbol{Q}_{\mathrm{SW}}$ or $\delta\boldsymbol{Q}_{\mathrm{Rus}}$ instead of $\delta\boldsymbol{Q}_{\mathrm{ST}}$ and show how we can lower the viscosity on shear waves without sacrificing the robustness of the scheme.

2. Adjustment of the numerical viscosity

To investigate and adjust the numerical viscosity of the central pressure flux, it is important to keep in mind that for any contact wave, shear or entropy wave, there is no jump in the pressure nor in the normal velocity u. As a consequence, in that case, in (5) all but the third component of $\delta \boldsymbol{Q}_{ST}$ vanish. The third component only vanishes if there is no shear flow, i. e. no jump in the tangential velocity v. This means that the original AUFS-scheme [2] exactly resolves any pure entropy wave but no pure nontrivial shear wave. As already mentioned in the introduction, for a flux vector splitting scheme, it would be desirable to have it the other way: exact resolution of pure shear waves but not of pure entropy waves. In this way one could achieve both, nice resolution of boundary layers and positivity of the scheme at the same time.

The way to retain the positivity of the scheme is quite simple: replace the original viscosity $\delta \boldsymbol{Q}_{ST}$ (5) of the AUFS-scheme by the Steger-Warming viscosity $\delta \boldsymbol{Q}_{SW}$ (2) or the Rusanov viscosity $\delta \boldsymbol{Q}_{Rus}$ (6). As can be seen in Section 3, the price for the positivity is not too high. The loss in the overall accuracy is acceptable. If we use the Steger-Warming viscosity $\delta \boldsymbol{Q}_{SW}$, we even gain a much better resolution of shear waves. This can be seen in the results of Section 3.6.

To reduce the viscosity on shear waves, a first idea would be to replace the viscosity for the pressure flux by a HLLC-type viscosity as it is shown in Appendix A. Unfortunately, this would not only reduce the viscosity on the shear waves but also on entropy waves. They would be resolved exactly, again leading to lack of positivity and an unstable scheme. The solution of our problem is to use a weighted mean of the Rusanov- or Steger-Warming-viscosity with the HLLC-viscosity, e. g.

$$\delta \boldsymbol{Q} = \theta \, \delta \boldsymbol{Q}_{Rus} + (1 - \theta) \, \delta \boldsymbol{Q}_{HLLC} \,, \tag{7}$$

where $\boldsymbol{Q}_{HLLC}$ is taken from (A.21) with $S = \bar{c}$. One might be tempted to use the residual in the Rankine-Hugoniot condition for waves travelling with speed u as an indicator for shear waves as we did it in our carbuncle corrected HLLEM-solver HLLEMCC [5]. But that indicator is not able to distinguish between shear end entropy waves. Furthermore, in the context of a FVS-method, one would want to resort to an indicator that can be obtained with less computational effort.

For both, entropy and shear waves, there is no jump in the pressure nor in the normal velocity u. In addition, for pure entropy waves there is no jump

in the transverse velocity v, and for pure shear waves, there is no jump in the density. Thus, we chose as an indicator

$$\theta = \left(\frac{1}{3} \left(\frac{|p_l - p_r|}{p_l + p_r} + \frac{|u_l - u_r|}{|u_l| + |u_r|} + \frac{|\rho_l - \rho_r|}{\rho_l + \rho_r} \right) \right)^\alpha \quad \text{with} \quad \alpha \in [0, 1) \,. \tag{8}$$

In principle, it would be possible to use any other monotone increasing function h that maps $[0, 1]$ unto $[0, 1]$ instead of $(\cdot)^\alpha$. But numerical tests with piecewise linear functions indicate that we need $h(\xi) \to \infty$ as $\xi \to 0$ to get reasonable results.

3. Numerical results

As numerical tests, we employ only two-dimensional examples. To test the solvers for the carbuncle, we chose Dumbser's aforementioned steady shock test [4], the colliding flow problem proposed by LeVeque [6, Section 7.7], and the famous Quirk-test [7]. To test the resolution of entropy- and shear-waves, we employ a Gaussian pulse in the pressure and a Kelvin-Helmholtz instability.

As point of comparison, we give results computed with our HLLEMCC-scheme [5], a much more elaborate and, thus, more expensive scheme, which, at the one hand, prevents the breakdown of discrete shock profiles, but, on the other hand, still gives the exact flux for all linear waves, i. e. for both, shear and entropy waves. Wherever possible, we also show results of the original AUFS-scheme. For two tests, the steady shock and the colliding flow problem, this is not possible, since the scheme quite soon fails due to the lack of positivity.

3.1. Parameters for the tested schemes

To perform numerical tests, we first have to fix the parameters in the schemes: $\bar{u}$, $\bar{c}$, M, and α. For the averaged velocity $\bar{u}$ and the estimate for the Mach-number M we stick to the original settings of Sun and Takayama. For $\bar{u}$, we just take the arithmetic mean of u_l and u_r. The Mach-number estimate is given by

$$M = \begin{cases} \dfrac{\bar{u}}{\bar{u} - \min\{0, u_l - c_l, \hat{u} - \hat{c}\}} \,, & \text{if } \bar{u} > 0 \,, \\[2ex] \dfrac{\bar{u}}{\bar{u} - \max\{0, u_r + c_r, \hat{u} + \hat{c}\}} \,, & \text{if } \bar{u} \le 0 \,, \end{cases} \tag{9}$$

where the values with the hat are the isentropic approximations

$$\hat{u} = \frac{1}{2}(u_l + u_r) + \frac{c_l - c_r}{\gamma - 1} \,, \tag{10}$$

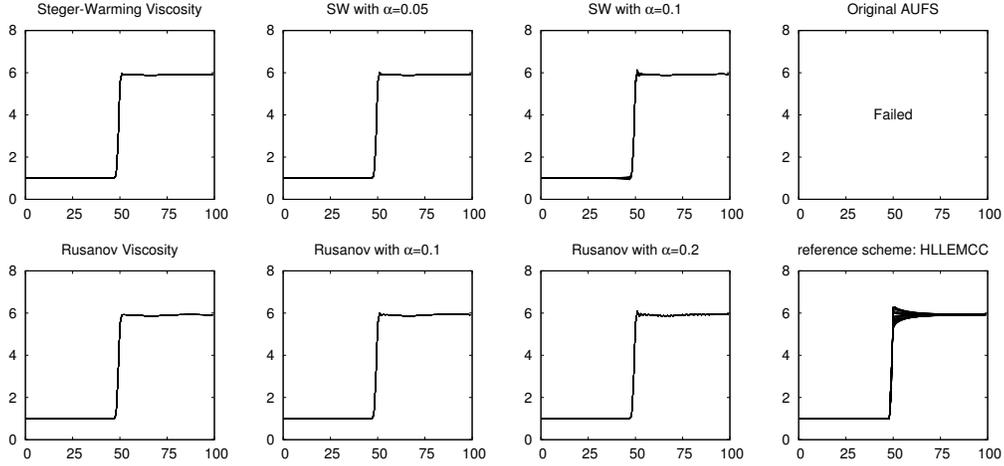$$\hat{c} = \frac{1}{2}(c_l + c_r) + \frac{1}{4}(\gamma - 1)(u_l - u_r) \tag{11}$$

Figure 2: Scatter plot of density for steady shock at time $t = 1000$ for different numerical viscosities; HLLEMCC as reference scheme.

with the gas constant γ. For the Steger-Warming viscosity $\delta \boldsymbol{Q}_{\text{SW}}$, we take $\bar{c}$ as the arithmetic mean of c_l and c_r, for the Rusanov viscosity $\delta \boldsymbol{Q}_{\text{Rus}}$ and the HLLC-viscosity $\delta \boldsymbol{Q}_{\text{HLLC}}$, we take it to be their maximum. For α, we test different settings: In the Steger-Warming case $\alpha = 0.05$ and $\alpha = 0.1$, in the Rusanov case $\alpha = 0.1$ and $\alpha = 0.2$.

3.2. Steady shock test

The steady shock problem was introduced by Dumbser et al. [4] as test for the carbuncle. We consider the worst case: The shock is located directly on a cell face. According to Dumbser et al. [4] this situation is most likely to evolve a carbuncle-like structure. We add artificial numerical noise of amplitude 10^{-6} to the primitive variables in the initial state. The results in Figure 2 show that, except for the original AUFS, which fails due to the lack of positivity, all variants nicely reproduce the steady shock, even at time $t = 1000$. The oscillations alongside the shock are even smaller than in the reference scheme.

3.3. Colliding flow

LeVeque [6, Section 7.7] outlined a test problem for the carbuncle instability. It consists of a pair of slowly moving shocks, initialised by a strong colliding flow. To trigger the carbuncle, LeVeque disturbs the initial state in one grid point. In this study we superimpose artificial numerical noise of amplitude 10^{-6} onto
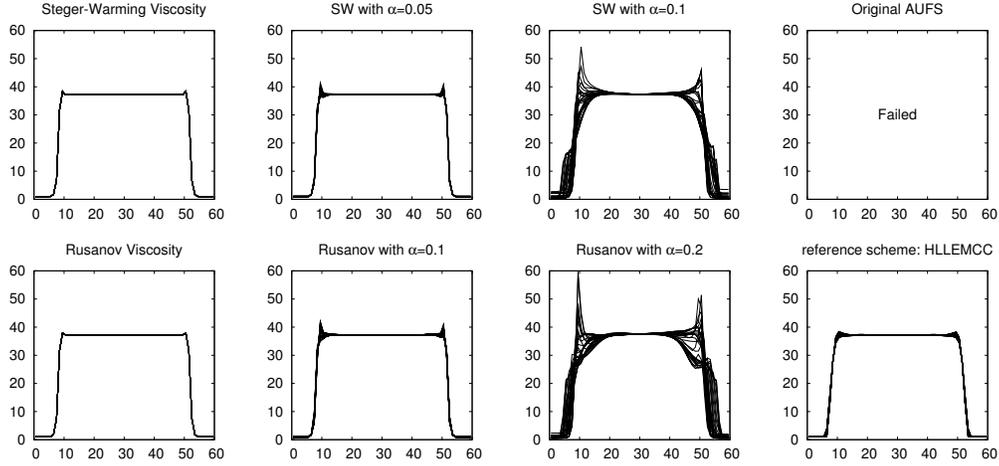
6

Figure 3: Scatter plot of density for Colliding flow at time $t = 40$ for different numerical viscosities; HLLEMCC as reference scheme.

the initial state instead of disturbing it in just one point. The noise is generated randomly. This allows us to make sure that the resulting structure of the solution is independent of the initial perturbation. For this test, we find in Figure 3 that lowering the viscosity leads to increasing overshoots near the shocks and, for $\alpha = 0.1$ in the Steger-Warming case and $\alpha = 0.2$ in the Rusanov case, even to a breakdown of the shock structure, a carbuncle.

3.4. Quirk test

Quirk [7] introduced a test problem which is known as Quirk-test. Contrary to the preceding example, it is not a one-dimensional Riemann problem, but consists of a shock running down a duct. The shock is caused by Dirichet-type boundary conditions on the left boundary. Originally, a disturbance of the middle grid line was used to trigger the instability [7]. Because the computations are done with a Cartesian code, we instead use numerical noise in the same manner as for the steady shock and the colliding flow problem. The only difference lies in the amplitude of the perturbation, here 10^{-3}. Although one would expect the Quirk test to be the hardest one, Figure 4 clearly shows that for this type of schemes, there is no difficulty in reproducing the running shock perfectly, even with the original AUFS-flux.
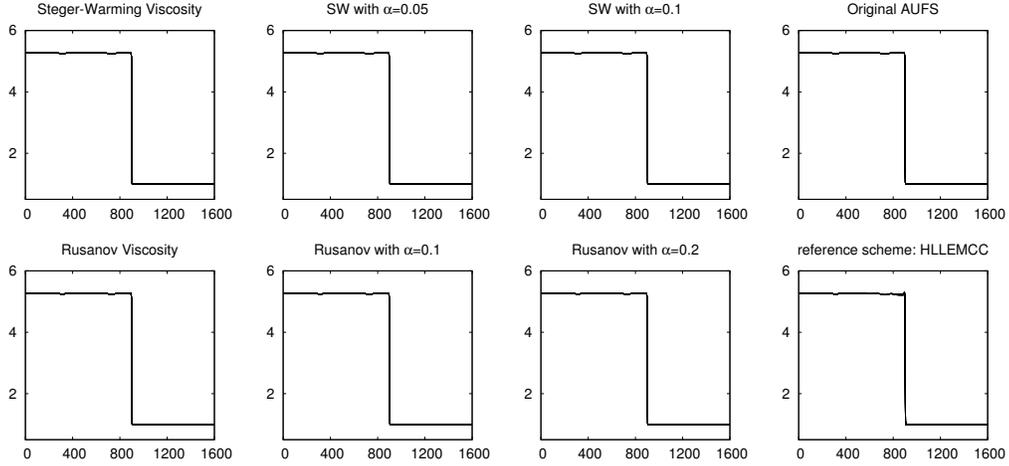
Figure 4: Scatter plot of density for Quirk test for different numerical viscosities; HLLEMCC as reference scheme.

3.5. Gauss pulse 2d

To test the schemes ability to resolve entropy waves, we start with a Gauss pulse with amplitude 1 and width 6 in the pressure, constant density $\rho = 1$ and zero velocity. The background pressure is $p_0 = 1$. Since the problem does not include any shear flow, it is a good test for the resolution of entropy waves. The results in Figure 5 mark that the loss in resolution compared to the original AUFS-scheme is visible. While the original AUFS-scheme yields a resolution that is in the range of the reference scheme, the modified versions all add much more viscosity on entropy waves.

3.6. Kelvin-Helmholtz instability

For the Kelvin-Helmholtz instability, we start with a flow which consists of three parts. In a region close to the middle line, it is uniformly directed to the left. Atop and below, it is directed in the opposite direction. Pressure and density are constant everywhere. To trigger the instability, we slightly disturb the y-component of the flow-velocity. Since for a first order scheme on our given 100×100-grid we cannot expect the instability to evolve, we resort to a second order scheme with direction-wise minmod on primitive variables. As the results in Figure 6 show, this test reveals a severe deficiency of the original AUFS-scheme: The viscosity on shear waves is even higher than with the Steger-Warming viscosity $\delta \boldsymbol{Q}_{\text{SW}}$. For $\alpha = 0.1$ in the Steger-Warming case and $\alpha = 0.2$ in
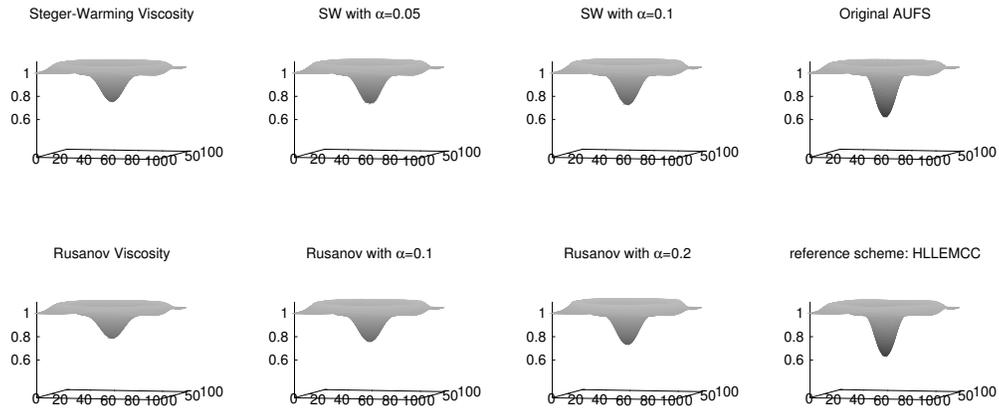
8

Figure 5: Density plot for Gauss pulse at time $t = 30$ for different numerical viscosities on the pressure flux; HLLEMCC as reference scheme.
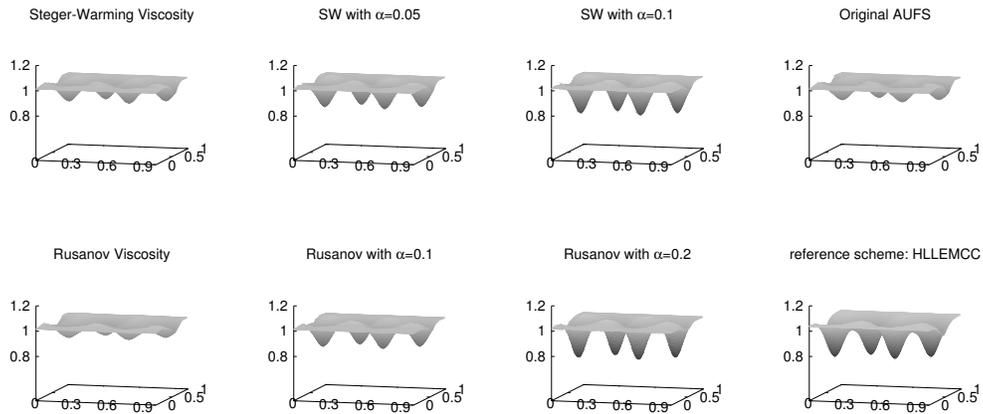

Figure 6: Density plot for Kelvin-Helmholtz instability at time $t = 4$ for different numerical viscosities on the pressure flux; HLLEMCC as reference scheme.

the Rusanov case, the results of the modified schemes are even in the range of those for the reference scheme.

4. Conclusions and outlook

We showed that, although the original AUFS-scheme by Sun and Takayama [2] lacks positivity and good resolution of shear layers, by some easy modifications, it is possible make it into a reliable scheme without breakdown of discrete shock profiles—usually called carbuncle—but with a good resolution of shear waves. This was done by replacing their tricky numerical viscosity on the central part by standard viscosities and weighting these with the viscosity of a HLLC-type solver for the pressure flux. The indicator used for the weights is based on the relative jumps in pressure, normal velocity and density.

In this paper, we started from the splitting (1). But there are many other possibilities to split the Euler flux into an advective and a pressure dominated part, e. g. the newly introduced splitting by Vázquez-Cendón and Toro [8], where all pressure terms are shifted to the right part and only the kinetic energy is left in the advective part, thus, the splitting of the energy flux becomes $u[\frac{1}{2}\rho \boldsymbol{v}^2] + \frac{\gamma}{\gamma-1}pu$. But all these splittings have in common that the Steger Warming and Rusanov viscosities $\delta \boldsymbol{Q}_{\mathrm{SW}}$ and $\delta \boldsymbol{Q}_{\mathrm{Rus}}$ no longer coincide for isentropic gases. Furthermore, the eigenvalues of the Jacobian of the pressure flux are no longer symmetric to zero. This means that, concerning the discretization of the pressure flux, many new questions arise which are beyond the scope of this work.

But, as can be seen from our numerical results, with the given splitting, it is already possible to construct a numerical scheme that is reliable, of low cost, and suits to many practical applications, both, in engineering and in computational physics.

Acknowledgements

Appendix A. HLLC-solver for pressure flux

Here we give the derivation of the HLLC-type numerical viscosity used for the reduction of the viscosity on shear waves in Section 2. Although we are mainly interested in 2d, we start with the 1d case. The 2d case then turns out to be only a slight modification.

Appendix A.1. Intermediate states

Since the eigenvalues of the Jacobian of $\boldsymbol{P}$ are 0 and $\pm \frac{\gamma-1}{\gamma} c$ with speed of sound c, the speed of the middle wave is always zero, and the formulas for the HLLC-scheme [9, Section 10] may be simplified. With $S_L \leq 0 \leq S_R$ being the bounding speeds for the Riemann problem and $\boldsymbol{q}_l^*, \boldsymbol{q}_r^*$ the left and right intermediate states, they read as

$$
\begin{aligned}
S_R \boldsymbol{q}_r^* - S_L \boldsymbol{q}_l^* &= S_R \boldsymbol{q}_r - S_L \boldsymbol{q}_l + \boldsymbol{f}(\boldsymbol{q}_l) - \boldsymbol{f}(\boldsymbol{q}_r) \\
&= (S_R - S_L) \boldsymbol{q}_{\mathrm{HLL}} ,
\end{aligned}
\tag{A.1}
$$

where the subscript HLL denotes the intermediate state of the according standard HLL-solver.

For the density equation, we get

$$
S_R \rho_r^* - S_L \rho_l^* = S_R \rho_r - S_L \rho_l .
\tag{A.2}
$$

To satisfy this independently from the special choice of S_L, S_R, we have to set

$$
\rho_l^* = \rho_l , \qquad \rho_r^* = \rho_r .
\tag{A.3}
$$

If we use the physical condition

$$
u_l^* = u_r^* = u^* ,
\tag{A.4}
$$

the momentum component of (A.1) can be simplified to

$$
(S_R \rho_r - S_L \rho_l) \, u^* = (S_R - S_L)(\rho u)_{\mathrm{HLL}} .
\tag{A.5}
$$

From that, we easily conclude

$$
\begin{aligned}
u^* &= (\rho u)_{\mathrm{HLL}} \cdot \frac{S_R - S_L}{S_R \rho_r - S_L \rho_l} \\
&= \frac{(\rho u)_{\mathrm{HLL}}}{\rho_{\mathrm{HLL}}} \\
&= u_{\mathrm{HLL}} .
\end{aligned}
\tag{A.6}
$$

For the energy equation, the HLLC-condition (2) is just

$$
S_R E_r^* - S_L E_l^* = (S_R - S_L) E_{\mathrm{HLL}} .
\tag{A.7}
$$

If we apply the ideal gas law and the physical condition

$$p_l^* = p_r^* = p^* \,, \tag{A.8}$$

and collect on the left hand side multiples of u^* and p^*, we find

$$p^* \frac{S_R - S_L}{\gamma - 1} + \frac{1}{2} u^{*2} (S_R \rho_r - S_L \rho_l) = (S_R - S_L) E_{\text{HLL}} \,. \tag{A.9}$$

If we now shift the u^*-terms to the right hand side and divide on both sides by $\frac{S_R - S_L}{\gamma - 1}$, we find

$$
\begin{aligned}
p^* &= (\gamma - 1) E_{\text{HLL}} - \frac{\gamma - 1}{2} u^{*2} \rho_{\text{HLL}} \\
&= (\gamma - 1) \left(E_{\text{HLL}} - \frac{1}{2} \rho_{\text{HLL}} u_{\text{HLL}}^2 \right) \\
&= p_{\text{HLL}} \,.
\end{aligned} \tag{A.10}
$$

Appendix A.2. Numerical Flux

For vanishing speed of the middle wave in the HLLC-solver, the according flux is

$$
\begin{aligned}
\boldsymbol{g}_{\text{HLLC}}(\boldsymbol{q}_l, \boldsymbol{q}_r) &= \boldsymbol{f}(\boldsymbol{q}_l) - S_L(\boldsymbol{q}_l - \boldsymbol{q}_l^*) \\
&= \boldsymbol{f}(\boldsymbol{q}_r) - S_R(\boldsymbol{q}_r - \boldsymbol{q}_r^*) \\
&= \frac{1}{2} \left(\boldsymbol{f}(\boldsymbol{q}_l) + \boldsymbol{f}(\boldsymbol{q}_r) \right) - \frac{1}{2} (S_L \boldsymbol{q}_l + S_R \boldsymbol{q}_r) + \frac{1}{2} (S_L \boldsymbol{q}_l^* + S_R \boldsymbol{q}_r^*) \,.
\end{aligned} \tag{A.11}
$$

Due to (A.3), the numerical mass flux vanishes. We only need to evaluate (A.11) for the momentum and energy flux.

Appendix A.2.1. Momentum flux

The momentum flux may be simplified by using the fact that

$$\left(S_L (\rho u)_l^* + S_R (\rho u)_r^* \right) - \left(S_L (\rho u)_l + S_R (\rho u)_r \right) = S_L \rho_l (u^* - u_l) + S_R \rho_r (u^* - u_r) \,, \tag{A.12}$$

and, thus, reads as

$$g_{\text{HLLC}_{\rho u}} = \frac{1}{2} (p_l + p_r) - \frac{1}{2} S_L \rho_l (u^* - u_l) - \frac{1}{2} S_R \rho_r (u^* - u_r) \,. \tag{A.13}$$

Appendix A.2.2. Energy flux

If we take into consideration that

$$
\begin{aligned}
S_L E_l^* + S_R E_r^* &= S_L\Big(\frac{p^*}{\gamma - 1} + \frac{1}{2}\rho_l u^{*2}\Big) + S_R\Big(\frac{p^*}{\gamma - 1} + \frac{1}{2}\rho_r u^{*2}\Big) \\
&= \frac{S_L + S_R}{\gamma - 1} p^* + \frac{1}{2}u^{*2}\left(S_L\rho_l + S_R\rho_r\right)
\end{aligned}
\tag{A.14}
$$

and use this to simplify the last bracketed term in (A.11), we find for the contribution of the acoustic system to the numerical energy flux

$$
g_{\mathrm{HLLC}_E} = \frac{1}{2}\left(p_l u_l + p_r u_r\right) - \frac{1}{2}\left(S_L E_l + S_R E_r\right) + \frac{1}{2}\frac{S_L + S_R}{\gamma - 1} p^* + \frac{1}{4}u^{*2}\left(S_L\rho_l + S_R\rho_r\right).
\tag{A.15}
$$

Appendix A.2.3. The case of symmetric bounding speeds

In the case of symmetric bounding speeds, i. e. $S_R = -S_L = S$, the momentum flux simplifies to

$$
g_{\mathrm{HLLC}_{\rho u}} = \frac{1}{2}\left(p_l + p_r\right) - \frac{S}{2}\Big(\rho_l\left(u^* - u_l\right) - \rho_r\left(u^* - u_r\right)\Big)
\tag{A.16}
$$

and the energy flux to

$$
g_{\mathrm{HLLC}_E} = \frac{1}{2}\left(p_l u_l + p_r u_r\right) + \frac{S}{2}\left(E_l - E_r\right) - \frac{S}{4}u^{*2}\left(\rho_l - \rho_r\right).
\tag{A.17}
$$

The intermediate pressure term p^* completely drops out.

Appendix A.3. Generalization to 2d

In 2d, for the second component of the momentum, we get by using (A.3)

$$
S_R\rho_r(v_r^* - v_r) = S_L\rho_l(v_l^* - v_l).
\tag{A.18}
$$

By an argument similar to that for the density, we conclude from that

$$
v_l^* = v_l, \qquad v_r^* = v_r.
\tag{A.19}
$$

Due to (A.19), not only the numerical mass flux, but also the transverse momentum flux vanishes. Another consequence of (A.19) together with (A.3) is that in the first line of (A.1), when written down for the 2d energy equation, all

13

ρv^2-terms cancel out. Thus, we are left with the 1d-version of that equation. As a consequence, we find that

$$p^* = p_{\text{HLL}_{1d}} \, . \tag{A.20}$$

In the end, the 2d numerical flux is exactly the same as the 1d flux with an additional zero component for the transverse momentum, and for the numerical viscosity, we find in the case of symmetric bounding speeds

$$\delta \boldsymbol{Q}_{\text{HLLC}_{\text{sym}}} = \frac{S}{2} \begin{pmatrix} 0 \\ \rho_l \, (u^* - u_l) - \rho_r \, (u^* - u_r) \\ 0 \\ (E_l - E_r) - \frac{1}{2} \, u^{*2} \, (\rho_l - \rho_r) \end{pmatrix} \, . \tag{A.21}$$

References

[1] J. L. Steger, R. Warming, Flux vector splitting of the inviscid gasdynamic equations with application to finite-difference methods., J. Comput. Phys. 40 (1981) 263–293. doi:10.1016/0021-9991(81)90210-2.

[2] M. Sun, K. Takayama, An artificially upstream flux vector splitting scheme for the Euler equations., J. Comput. Phys. 189 (1) (2003) 305–329. doi:10.1016/S0021-9991(03)00212-2.

[3] J. Gressier, P. Villedieu, J.-M. Moschetta, Positivity of flux vector splitting schemes., J. Comput. Phys. 155 (1) (1999) 199–220. doi:10.1006/jcph.1999.6337.

[4] M. Dumbser, J.-M. Moschetta, J. Gressier, A matrix stability analysis of the carbuncle phenomenon., J. Comput. Phys. 197 (2) (2004) 647–670. doi:10.1016/j.jcp.2003.12.013.

[5] F. Kemm, A carbuncle free Roe-type solver for the Euler equations., Benzoni-Gavage, Sylvie (ed.) et al., Hyperbolic problems. Theory, numerics and applications. Proceedings of the 11th international conference on hyperbolic problems, Ecole Normale Supérieure, Lyon, France, July 17–21, 2006. Berlin: Springer. 601–608 (2008). (2008).

[6] R. J. LeVeque, Nonlinear conservation laws and finite volume methods, in: O. Steiner, A. Gautschy (Eds.), Computational Methods for Astrophysical Fluid Flow, Springer, Berlin, Heidelberg, 1998, pp. 1–160.

[7] J. J. Quirk, A contribution to the great Riemann solver debate., Int. J. Numer. Methods Fluids 18 (6) (1994) 555–574. doi:10.1002/fld.1650180603.

[8] M. E. Vázquez-Cendón, E. F. Toro, A flux vector splitting scheme for the euler equations, Presentation at Numerical Methods for Hyperbolic Equations: Theory an Applications. An international conference to honour Professor E.F. Toro, University of Santiago de Compostela, 4-8 July 2011, Spain.

[9] E. F. Toro, Riemann solvers and numerical methods for fluid dynamics. A practical introduction. 3rd ed., Berlin: Springer, 2009. doi:10.1007/b79761.